processes

MDPI

Article

Research on AGC Nonlinear Compensation Control for Electro-Hydraulic Servo Pump Control of a Lithium Battery Pole Strip Mill

Kai Wang [1], Gexin Chen [1,2,*], Cheng Zhang [1], Keyi Liu [2] and Fei Wang [1,2]

1 School of Mechanical Engineering, Yanshan University, Qinhuangdao 066004, China; kaiwang@stumail.ysu.edu.cn (K.W.); chengz@stumail.ysu.edu.cn (C.Z.); wf69@xjie.edu.cn (F.W.)

2 Mechanical and Electrical Engineering, Xinjiang Institute of Engineering, Urumqi 830023, China; lky@xjie.edu.cn

* Correspondence: jygxchen@ysu.edu.cn; Tel.: +86-0991-7977195

Abstract: Electrode roll forming involves rolling a battery electrode into a preset thickness using a hydraulic roll gap thickness automatic control system (hydraulic AGC for short). The pump-controlled AGC is a highly nonlinear servo system, which is a combination of mechanical, hydraulic and electronic control disciplines; thus, as a new technology, it still faces many challenges in the field of pole plate rolling. In this paper, electro-hydraulic servo pump-controlled AGC technology is replaced by electro-hydraulic servo valve-controlled AGC technology. With pump-controlled AGC high-precision thickness control as the research objective, the fuzzy control method is selected to deal with complex nonlinear systems based on pump-controlled AGC nonlinear stiffness characteristics and nonlinear transmission characteristics. A characteristic compensation control strategy is proposed. At the same time, considering the load fluctuation caused by the uneven thickness of the electrode plate under the intermittent coating rolling condition of a lithium battery, the fuzzy internal model (IMC) compensation control strategy was proposed to compensate the structural characteristics of the electrode plate rolling. Comparative experiments show that the position control accuracy of the pump-controlled AGC system can be improved significantly by using a fuzzy IMC compensation control strategy. The steady-state accuracy of the slope signal can reach ±0.7 μm, and the position-following accuracy of the sinusoidal signal can reach ±1.8 μm. In addition, this study will assist technological upgrades to lithium battery electrode roll forming and fixed-roll-gap rolling, laying a theoretical foundation for the promotion of pump control technology in the field of electrode rolling.

Keywords: pole rolling; electro-hydraulic servo pump control; nonlinear drive; compensation control; fuzzy internal model

Citation: Wang, K.; Chen, G.; Zhang, C.; Liu, K.; Wang, F. Research on AGC Nonlinear Compensation Control for Electro-Hydraulic Servo Pump Control of a Lithium Battery Pole Strip Mill. *Processes* **2024**, *12*, 158. https://doi.org/10.3390/pr12010158

Academic Editor: Dan Zhang

Received: 25 November 2023
Revised: 27 December 2023
Accepted: 30 December 2023
Published: 9 January 2024

1. Introduction

As the power source of new energy vehicles, lithium batteries account for about 40% of the cost of new energy vehicles, and their performance stability also determines the safety and driving range of the vehicle [1]. The roll forming of positive and negative electrode sheets of lithium batteries is one of the key processes, which has a great impact on the battery's use and safety performance. The manufacturing process is shown in Figure 1. Electrode sheet rolling involves the application of a uniform mixture of electrical compound slurry on copper foil or aluminum foil and other substrates and it compacts the electrical slurry particles on the electrode sheet through rolling, thereby increasing the compaction density of the battery electrode sheet. Therefore, electrode sheet rolling not only decreases the thickness of the electrode sheet but also changes the compaction density of the electrode sheet. After rolling, the compaction density of the pole sheet is either too small or too large, resulting in the polarization phenomenon or battery voltage reduction and capacity reduction, which is not conducive to battery use. Therefore, electrode plate rolling has a crucial effect on the production of the electrode plate and the performance of the battery.

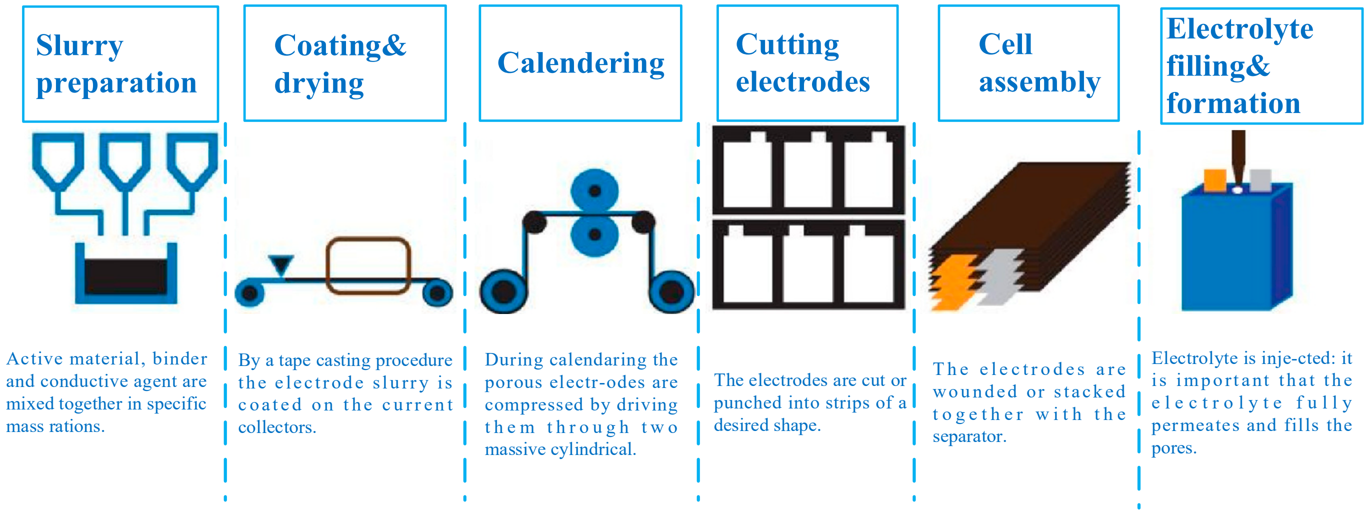

Figure 1. Process flow chart.

Rolling changes the compaction density of the battery's electrode coating. In a certain range, the smaller the thickness of the electrode sheet when rolled, the higher the compaction density of the electrode sheet will be, and so the gap between the active material inside the electrode coating becomes smaller; the larger the contact area, the larger the ion conductive path and bridge, thus reducing the internal resistance of the lithium battery. If the compaction density further increases beyond the normal range, this will lead to the contact density of the active material particles in the coating being too tight, although this will both increase the electronic conductivity and reduce or block the lithium ion channel, so that the battery increases the polarization phenomenon during discharge, and will eventually cause the battery voltage to decrease and the battery capacity to decrease. On the contrary, if the compaction density of the electrode plate is too small, the distance between the active material particles in the electrode plate coating will be large. Although the lithium ion channel is relatively smooth, it enhances the movement of lithium ions inside the battery, but the excessive distance between the particles will affect the electronic conduction and can also easily cause polarization when the battery is discharged, which is not conducive to the use of the battery [2]. Therefore, electrode plate rolling has a crucial effect on the production of the electrode plate and the performance of the battery.

At present, the electrode rolling process of lithium batteries is usually completed by an electrode rolling mill, and the automatic control system of the hydraulic roll gap thickness (hydraulic AGC) is used to press the battery electrode sheet into a predetermined thickness under the rolling condition of a constant roll gap. Compared with valve-controlled AGC, pump-controlled AGC can not only effectively solve the inherent defects of valve-controlled cylinder technology itself, but also has the following advantages: (1) The use of pump-controlled technology can avoid the servo valve failure caused by the pollution of hydraulic oil by the external environment, reduce the cleanliness of the system oil (NAS7-9) and reduce the maintenance cost of the system. (2) The use of a pipeline-free connection in the pump control system can avoid oil leakage problems in the complex pipelines of the valve control system. (3) The pump control technology adopts the volume speed regulation form of the servo motor direct drive hydraulic pump output of hydraulic oil, eliminating the servo valve, hydraulic pipeline and pump station and other system components, using the integrated installation form, not only to avoid the overflow throttling loss and greatly reduce the area of the equipment, but also to improve the power-to-weight ratio of the system. In this paper, electro-hydraulic servo pump control cylinder technology is proposed to replace the original valve-controlled cylinder technology with inherent system defects, and it is applied in an AGC hydraulic system [2–10]. The unique technical advantages of pump control technology compared with valve control technology will help to upgrade and optimize the AGC system equipment of the pole plate mill. However, in the rolling process of the pole sheet, the pole strip and the hydraulic cylinder show nonlinear stiffness characteristics, and the pump control system is a highly nonlinear system, which will directly affect the high-precision rolling of the pole sheet [11–14]. Additionally, the control precision of the traditional PID algorithm is decreasing, so it is necessary to find a new control algorithm to replace the traditional PID algorithm. Moreover, the rolling precision of the pole plate should be controlled at ± 0.5 μm, which puts forward higher requirements for the high-precision control of hydraulic AGC.

With the continuous improvement of market requirements for the rolling accuracy and quality of polar sheets, more scholars have paid attention to the study of the nonlinear disturbances, nonlinear characteristics and microscopic compaction mechanisms of polar sheets in the rolling process [15–17] to further improve the forming quality of polar sheet thickness [18]. Antartis et al. from the University of Inoa in the United States conducted a hot equiaxial compression experiment on the electrode sheet and determined that the graphite negative electrode sheet has the best mechanical and electrochemical properties when the porosity is 45% [19]. Guan Yuming et al. [20] from Hebei University of Technology proposed an optimization scheme for the structure of the traditional roller press by establishing a mathematical model of the force on the active roller of the roller press, which improved the quality of the electrode rolling of lithium batteries. Zad et al., Iran [21], Chong CheeSoon et al., Technical University of Malaysia [22], and Masoumeh, University of Manitoba, Canada, Ren and Esfandiari et al. [23] proposed a sliding mode variable structure control strategy based on an independent switching structure, a fuzzy logic control strategy based on particle swarm optimization and a position controller based on fixed gain to achieve the goal of improving the position control accuracy, respectively. Cao Fulu of Xi'an Electronic Engineering Research Institute proposed a PID controller optimized based on a genetic algorithm for pump control and direct drive characteristics and verified that the controller had good dynamic response characteristics [24].

From the above research, it can be found that most scholars have adopted different control strategies to improve the control accuracy of the position control of the pump control system [25,26] and lack the characteristic analysis that takes a servo motor, drive shaft, hydraulic pump and hydraulic cylinder as the main line. The nonlinear rolling stiffness of the pole plate and the nonlinear spring stiffness of the hydraulic cylinder are composed of the nonlinear rolling stiffness of the pole plate, which affects the rolling thickness forming quality of the pole plate. The pump-controlled AGC hydraulic system has problems such as high nonlinearity and strong coupling [27,28], which lead to the thickness deviation of the electrode plate of the lithium battery after the completion of rolling, further affecting the service performance and safety performance of the lithium battery.

This paper takes pump-controlled AGC high-precision thickness control of a pole plate rolling mill as the research objective and the electro-hydraulic servo pump-controlled AGC system (pump-controlled AGC for short) as the research object to carry out characteristic compensation control research on the influence characteristics of the pole plate thickness control system. At the same time, considering the intermittent coating rolling condition of the lithium battery, the load fluctuation caused by the uneven thickness of the pole plate is taken into account. The high-precision control strategy of a pump-controlled pole strip mill is studied, the influence characteristics of the pole strip thickness control system are studied and a fuzzy IMC (internal model) compensation control strategy is proposed. The paper is organized as follows: Section 2 explores the stiffness characteristics between the hydraulic cylinder and the pole plate. Section 3 explores the nonlinear factors affecting the transmission of the pump-controlled AGC hydraulic system. In Section 4, the characteristic compensation control and structure compensation control are carried out for the electrode plate rolling thickness control system. In Section 5, the nonlinear compensation control strategy proposed above is experimentally studied according to the rolling condition of a pump-controlled pole plate mill with a fixed roll gap. The thesis is summarized in Section 6.

2. Study on Nonlinear Stiffness Characteristics of Pole Mill

2.1. Research on Nonlinear Stiffness Characteristics of Polar Plate

2.1.1. Theoretical Rolling Force Calculation of Pole Sheet

In the rolling process of the pole sheet, the rolling process of the pole sheet is generally divided into four regions according to the position of the pole sheet and the state of the pole sheet coating, which are, respectively, Zone I—collapse zone; Zone II—polar compression region; Zone III—intense compression zone; Zone IV—thickness rebound zone [29]. The polar sheet rolling process partition diagram is shown in Figure 2 (in order to clearly express the rolling process, the polar sheet rolling diagram in this paper is only a schematic diagram, and the actual rolled polar sheet thickness and roll diameter ratio is larger).

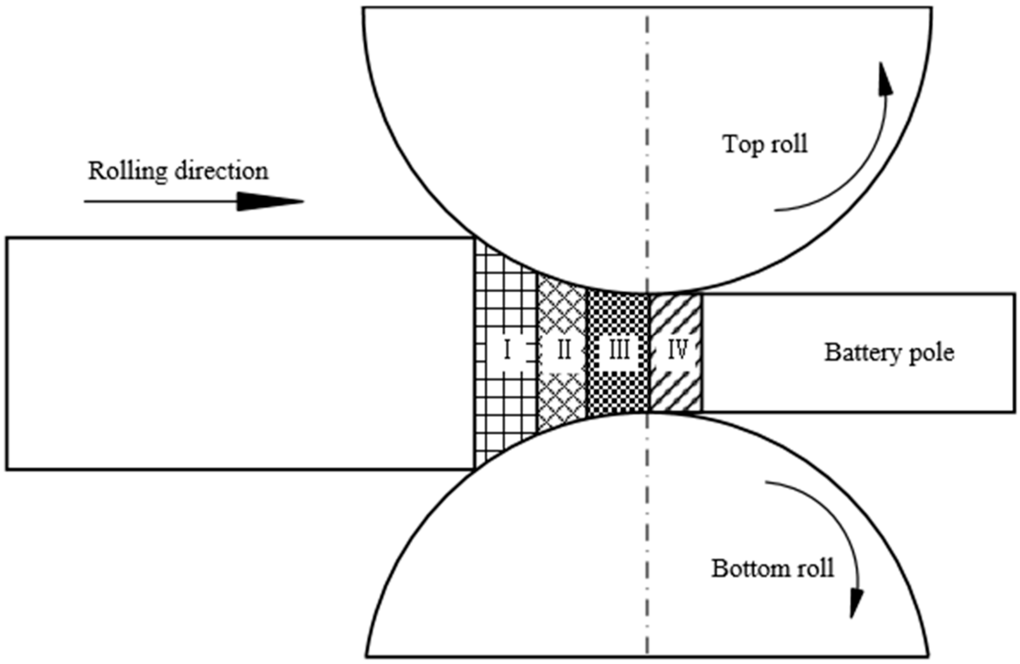

Figure 2. Schematic diagram of the rolling section of the battery pole plate.

The rolling force is one of the key parameters in the roll forming process of a polar sheet. The rolling force affects the working state of the roll under the rolling condition with a constant roll gap, and thus affects the quality of the roll forming.

The unit rolling force subjected to the pole sheet is:

$$P_L = R \times \sum_{1}^{m} \int_{\alpha_n}^{\alpha_{n+1}} P_r(\cos\alpha + \mu \sin\alpha)\mathrm{d}\alpha \tag{1}$$

where P_L is the unit rolling force (N) received by the pole strip; P_r is the unit rolling force on the electrode element (N); R is the radius of the roll; α is the bite angle (rad) corresponding to the polar plate element; μ is the ratio of the friction force between the electrode element and the roll to the unit rolling force applied to the electrode element; and m is the number of microelement regions of the polar slice.

By multiplying the unit rolling force with the width of the pole strip, the rolling force subjected to the pole strip can be obtained, so the size of the rolling force can be expressed as:

$$P = B \times P_L = B \times R \times \sum_{1}^{m} \int_{\alpha_\mathrm{n}}^{\alpha_{n+1}} P_r(\cos\alpha + \mu \sin\alpha)\mathrm{d}\alpha \tag{2}$$

2.1.2. Theoretical Calculation of Rolling Thickness of Pole Sheet

The Heckel formula is not applicable to brittle materials such as alumina, but the compression materials in this paper are mainly active substances, conductive agents, binder and other substrates, and the coating has a strong deformability. Therefore, the exponential relationship expressed by the Heckel equation can also be converted into the relationship between the forming thickness of the lithium battery electrode sheet and the unit rolling force, and the relationship expression is as follows:

$$h = h_{min} + (h_1 - h_{min})\exp\left(-\frac{P_L}{\gamma}\right) \tag{3}$$

where h_1 is the initial thickness (m) of the pole sheet before rolling; $h_{\min}$ is the minimum rolling thickness of the pole sheet roll, namely the thickness of the rolling seam (m); and γ is the parameter that characterizes the electrode plate pressure behavior, which can be equivalent to the reciprocal of the Heckel constant K.

The relationship between the rolling force and the forming thickness of the pole sheet is as follows:

$$K_m = \frac{P_L}{h_1 - h} = \frac{P_L}{\Delta h} \tag{4}$$

where K_m is the nonlinear stiffness of the pole plate (N/m) and Δh is the compression thickness (m) of the pole roll forming.

2.1.3. Simulation of Nonlinear Stiffness Characteristics of Polar Plate

The influence of roll deformation on the forming thickness of the pole sheet is not considered; that is, the elastic deformation of roll is not considered when the stiffness of roll is set to be large. Other parameter settings are shown in Table 1.

Table 1. Parameter setting.

Physical Name	Parameter	Unit
Roll diameter	600	mm
Roll body length	500	mm
Roll gap size	110	µm
Initial thickness of pole plate	165	µm
Polar sheet material	Graphite	-
Compressive impedance parameters	195	-

In this paper, ANSYS(2020R2) software was used to conduct simulation analysis with a graphite negative electrode sheet possessing compressive impedance parameters as the research object. By applying a 100–900 N/mm (whole hundred) force to the electrode sheet, the forming thickness of the electrode sheet was fitted with the relationship obtained in Formula (3), and the results are shown in Figure 3.

According to the analysis of Figure 3, there is an exponential relationship between the rolling force on the pole sheet and the rolling force on the pole sheet. The error values of the theoretical curve and the actual curve in the comparison figure are both within 10%. The size of the roll gap can be obtained according to the final forming thickness and initial thickness of the pole piece under the rolling condition of a constant roll gap.

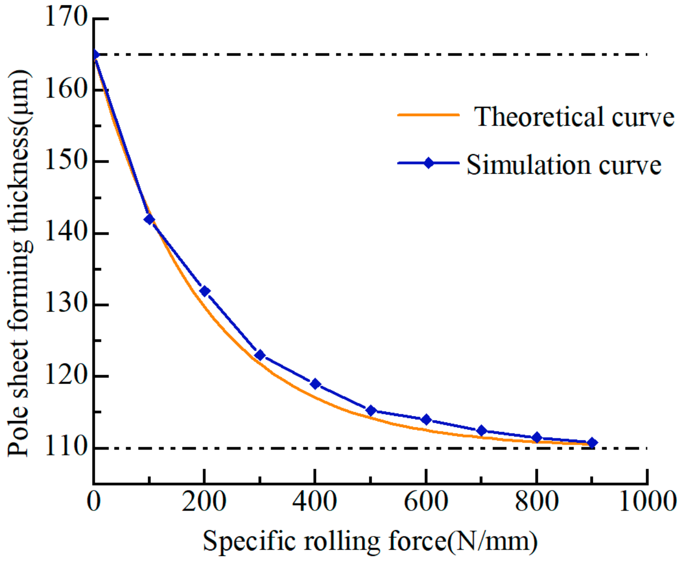

Figure 3. Rolling force-thickness relationship diagram.

2.2. Research on Nonlinear Stiffness Characteristics of Hydraulic Cylinder

When analyzing the influence of the hydraulic cylinder piston stiffness and hydraulic oil stiffness on the hydraulic spring stiffness, the piston can be approximately regarded as a rigid body, and only the stiffness of hydraulic oil has an effect on the hydraulic spring stiffness.

The total hydraulic spring stiffness of the hydraulic cylinder is composed of the two hydraulic spring stiffnesses of the left chamber and the right chamber of the hydraulic cylinder connected in parallel. The total hydraulic spring stiffness of the hydraulic cylinder K_h can be expressed as:

$$K_h = \alpha K_{h1}(x) + \gamma K_{h2}(x) = \alpha \frac{\beta_e A_1^2}{A_1 x + V_{L1}} + \gamma \frac{\beta_e A_2^2}{A_2(L-x) + V_{L2}} \tag{5}$$

α and γ in Formula (5) are undetermined coefficients. Through the analysis of Formula (5), it can be seen that the hydraulic spring stiffness K_h is closely related to the undetermined coefficients of nonlinear α and γ.

2.3. Nonlinear Stiffness Characteristic Analysis

The relationship between the hydraulic spring stiffness K_h, roll stiffness K_l and pole plate stiffness K_m is in series, so the expression of the nonlinear comprehensive stiffness K_g of pole plate rolling is as follows:

$$\frac{1}{K_g} = \frac{1}{K_h} + \frac{1}{K_l} + \frac{1}{K_m} \tag{6}$$

According to Formula (6), the total hydraulic spring stiffnesses of the hydraulic cylinder, roll stiffness and pole plate stiffness were coupled to form a nonlinear comprehensive stiffness of pole plate rolling. Further, the nonlinear stiffness characteristics of pole plate rolling were simulated and analyzed, and the simulation results are shown in Figure 4.

It can be seen from the analysis of Figure 4 that the nonlinear comprehensive stiffness of pole sheet rolling is smaller than the total hydraulic spring stiffness of the hydraulic cylinder, roll stiffness and pole sheet stiffness, and the nonlinear comprehensive stiffness of pole sheet rolling is mainly determined by the hydraulic spring stiffness and pole sheet rolling stiffness.

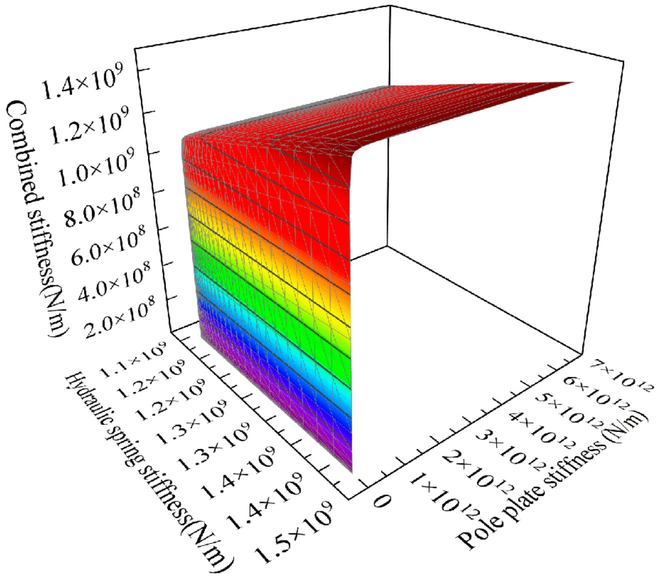

Figure 4. Comprehensive stiffness simulation diagram.

3. Research on Nonlinear Transmission Characteristics of Pump-Controlled AGC

3.1. Study on Transmission Characteristics of Motor Pump Group

3.1.1. Research on Low-Speed Characteristics of Servo Motor

The servo motor control mode of the pump-controlled AGC system adopts an $i_d = 0$ control method. When the pressure or position control of the pump control system reaches stability, the servo motor is usually controlled to drive the hydraulic pump to operate at a low-speed condition, and only maintain the oil leakage of the system, so it also puts higher requirements on the low-speed condition of the servo motor. When the motor increases from 0 r/min to 800 r/min in a short period of time, the speed of the motor has a slight overshoot, the maximum overshoot is 2.4% and the servo motor speed reaches the steady state at 0.13 s. The servo motor system shows better dynamic response characteristics and better steady-state control accuracy. When the system is disturbed by the load torque of 8 N·m at 0.2 s, the servo motor speed reaches the speed steady state at 0.27 s and the servo motor torque waveform also reaches the torque steady state at the corresponding time. The servo motor speed waveform diagram can be obtained as shown in Figure 5a and torque waveform diagram as shown in Figure 5b.

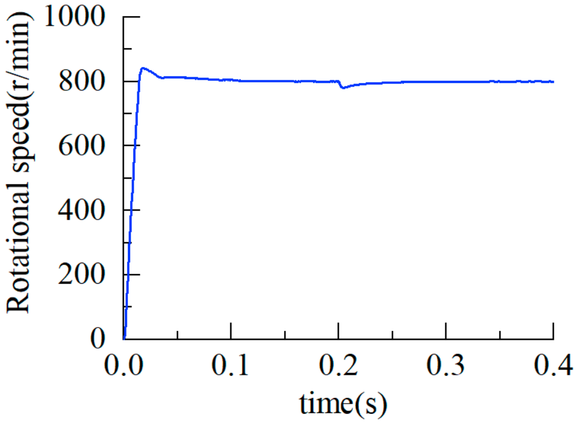

(**a**) Tachoscillogram.

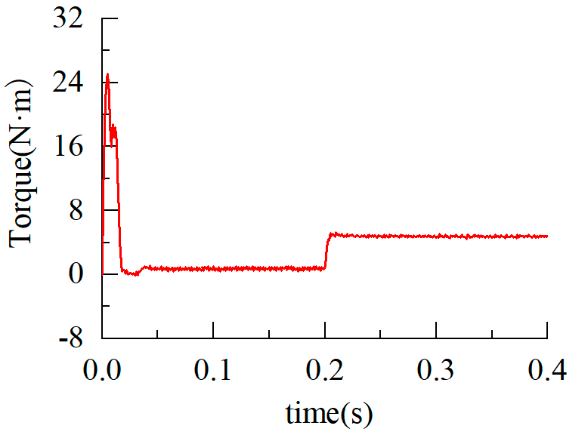

(**b**) Torque waveform diagram.

Figure 5. Servo motor simulation diagram.

By analyzing the simulation results shown in Figure 5, it can be concluded that the control parameters of the servo motor can ensure the dynamic and steady-state control accuracy of the system, and it also has good anti-interference ability, which can meet the performance requirements of the subsequent system on the servo motor.

3.1.2. Research on Flow Output Characteristics of Hydraulic Pump

Due to the existence of a certain amount of oil leakage and oil compression in the system, the pump-controlled AGC hydraulic system shows a hysterical phenomenon during startup and low-speed operation, which is called the dead zone of the system, and will lead to a reduction in the dynamic performance of the system and the control accuracy of the system [30]. Therefore, it is necessary to compensate the dead zone characteristics of the system.

The time when the hydraulic pump begins to input effective flow into the system was set to t_0, and the speed $n_p(t_0) = n_{p0}$ and pressure $p_p(t_0) = p_L$ were measured at this time. Formula (7) is the mathematical model of the hydraulic pump flow dead zone, namely:

$$n_{p0} = \frac{p_L}{K} + \frac{\tau}{K}\left[\frac{\mathrm{d}p_p(t)}{\mathrm{d}t}\right]_{t=t_0} \tag{7}$$

The first term on the right of the equation is the leakage term of the system; the second term on the right of the equation is the system compression term, where $\mathrm{d}p_p$ is the pressure change element (Pa) of the cavity; τ is the time constant; and K is the gain. The hydraulic pump flow dead zone node speed n_{p0} is numerically equal to the dead zone width of the one-way output flow of the hydraulic pump. The above research is aimed at unidirectional high-pressure quantitative pumps; thus, for bidirectional high-pressure hydraulic pumps, the dead zone range should be $-n_{p0} \sim n_{p0}$, as shown in Figure 6.

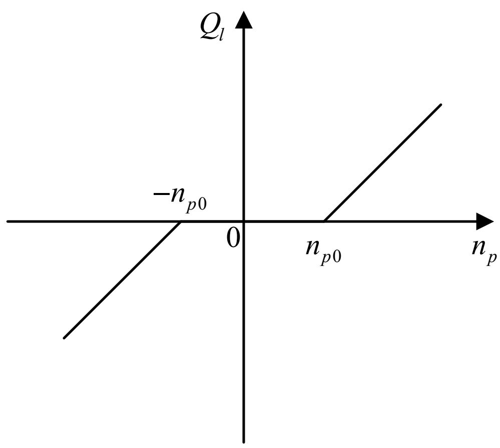

Figure 6. Hydraulic pump flow dead zone.

In order to verify the flow dead zone characteristics of the hydraulic pump, a hydraulic pump flow dead zone test platform of the pump control system was built to carry out a flow dead zone experiment on the hydraulic pump, and test the no-load flow and on-load flow of the system, respectively. The flow characteristic curves are shown in Figures 7 and 8, respectively. During the no-load flow test of the system, the load simulation adjustable throttle valve is fully opened. At this time, no load is in no-load state between the oil outlet and the oil inlet of the hydraulic pump of the electro-hydraulic pump control system. By changing the servo motor speed, the flow sensor is used to detect the no-load flow and leakage flow of EPU, respectively, and the no-load flow characteristic curve of the hydraulic pump can be obtained, as shown in Figure 7. When carrying out the system current-carrying test, the load analog adjustable throttle valve is completely closed, and the servo motor speed is given. When the system pressure reaches stability at this speed, the hydraulic pump still inputs the flow to the system, but the system pressure has been stable at this time, so the output flow of the hydraulic pump is the dead zone flow of the hydraulic pump under this pressure. The test results are shown in Figure 8.

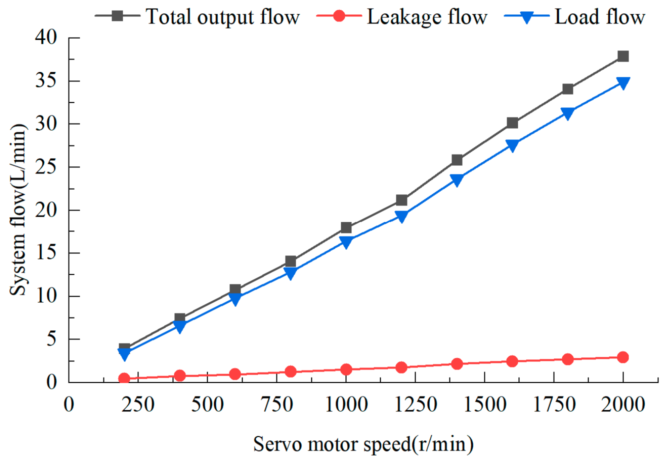

Figure 7. EPU no-load flow characteristic curve.

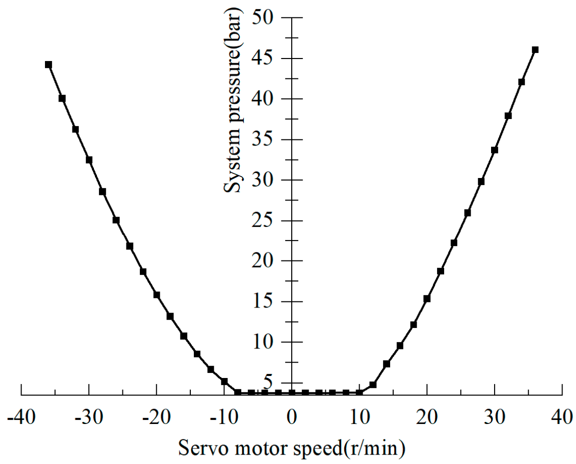

Figure 8. EPU load building voltage characteristic curve.

As can be seen from Figure 7, there is no flow output in the system when the rotational speed of the hydraulic pump is low, and this stage is the dead-zone stage of the hydraulic pump flow. With the increase in hydraulic pump speed, the leakage flow of the system increases. An analysis of Figure 8 shows that with a continuous increase in rotational speed, the system pressure gradually increases, resulting in the increase in system leakage, and the final system pressure tends to be stable. The output flow rate of the hydraulic pump provides the flow rate of oil leakage and compression under the current pressure, which is the flow dead zone of the hydraulic pump under the current pressure. To sum up, in order to ensure the thickness requirements of the final rolling of the pole sheet, it is necessary to control and compensate the output speed of the hydraulic pump to ensure the flow output of the hydraulic pump and improve the rolling accuracy of the pole sheet.

3.2. Research on Coupling Characteristics of Pump-Controlled Cylinder Drive System

The coupling characteristics of load pressure and load flow of the pump control cylinder drive system were simulated and analyzed, and the simulation curve was obtained as shown in Figure 9.

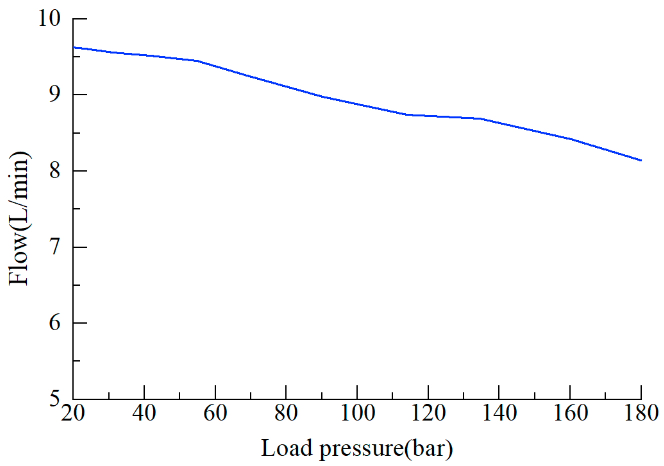

Figure 9. Simulation diagram of system pressure flow coupling characteristics.

As can be seen from the simulation results in Figure 9, when the load pressure of the system changes, the total leakage coefficient and the compressed amount of oil will also change, which will further affect the load flow output of the system, and to a certain extent, the load flow shows sagging attenuation characteristics. The droop attenuation characteristic of load flow will affect the pump-controlled AGC hydraulic cylinder position output, reduce the steady-state position control accuracy of the system and also reduce the pole roll forming quality.

4. Research on Pump-Controlled AGC High-Performance Thickness Control Strategy

4.1. Research on Characteristic Compensation

The servo motor speed required by the thickness rebound of pole plate rolling, along with the flow dead zone of the hydraulic pump, oil compression and oil leakage are compensated for by the compensation control method in real time. Because the pump control system is a servo motor direct-drive quantitative pump to produce speed output, so the pump control pole mill is involved in the rolling process, the servo motor speed compensation instructions are:

$$\begin{aligned} n_{pm} &= n_{p1} + n_{p2} + n_{p3} + n_{p4} \\ &= \frac{A_p \cdot \Delta h}{D_p} + \frac{p_L}{K} + \frac{\tau}{K}\left[\frac{\mathrm{d}p_p(t)}{\mathrm{d}t}\right]_{t=t_0} + \frac{V_t \dot{p}_L}{D_p \beta_e} + \frac{\left(C_{ip}+C_{ep}\right)p_L + C_T T}{D_p} \end{aligned} \tag{8}$$

where n_{pm} is the servo motor speed output command (rad/s) to compensate the characteristics of the pole plate rolling process; A_p is the working area of the hydraulic cylinder (m^2); $\Delta h'$ is the thickness rebound value (m); n_{p1} is the speed output of the hydraulic pump under thickness rebound compensation (rad/s); n_{p2} is the rotational speed output (rad/s) of the hydraulic pump under flow dead zone compensation; V_t is the hydraulic cylinder area (m^2); n_{p3} is the speed output of the hydraulic pump under oil compression compensation (rad/s); C_T is the leakage coefficient of system temperature action; T is the temperature of the hydraulic fluid of the system (°C); and n_{p4} is the rotational speed output (rad/s) of the hydraulic pump with oil leakage compensation.

4.2. Research on Fuzzy Internal Model Structure Compensation Control

In this paper, the fuzzy internal model control strategy was used to compensate the structural characteristics of pole plate rolling. Internal model control (IMC) is a new control strategy for controller design based on the process mathematical model [31]. Compared with traditional PID control, IMC can better solve the model uncertainty and external load interference in the system modeling process [32]. The fuzzy IMC control principle is shown in Figure 10.

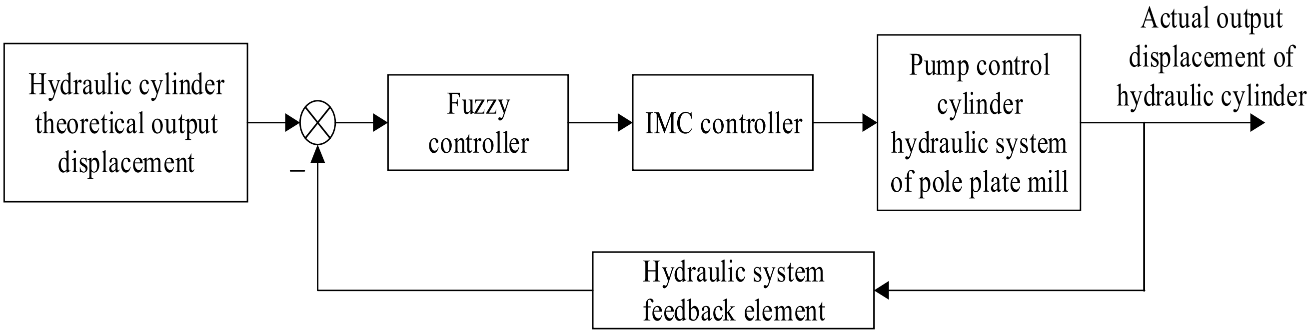

Figure 10. Fuzzy internal model control schematic diagram.

Combining fuzzy control with IMC control, the fuzzy IMC control algorithm was designed to improve the rolling precision of the pump-controlled pole plate mill. On the basis of characteristic compensation and a fuzzy IMC control strategy, the pump control AGC system of the pole plate mill was compensated, and the fuzzy IMC compensation controller was formed to ensure the control precision of the fixed-roll-gap rolling of the pole plate. The architecture of the fuzzy IMC compensation controller is shown in Figure 11.

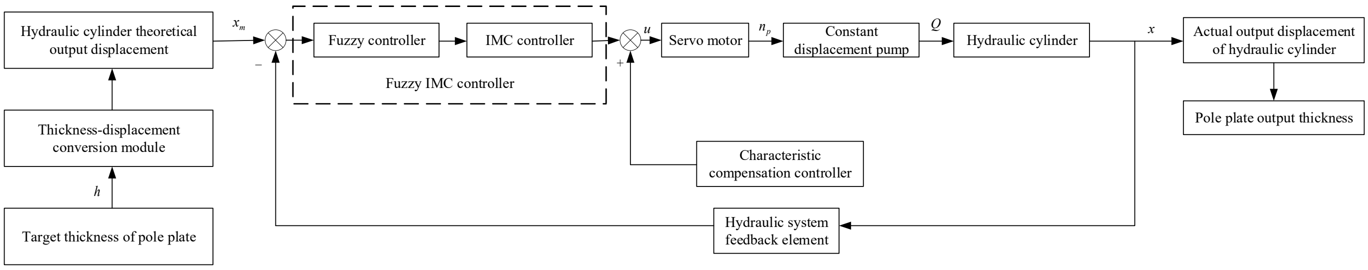

Figure 11. Fuzzy IMC compensation controller structure diagram.

The fuzzy IMC compensation controller and the traditional PID controller designed in this paper were simulated, and the simulation results were compared and analyzed. The internal structure simulation diagram of the IMC controller is shown in Figure 12. The output position error diagram of the hydraulic cylinder can be obtained by applying a slope signal with an initial value of 0~50 μm and a sinusoidal signal with an amplitude of 50 μm and frequency of 2 Hz to the system, as shown in Figures 13 and 14.

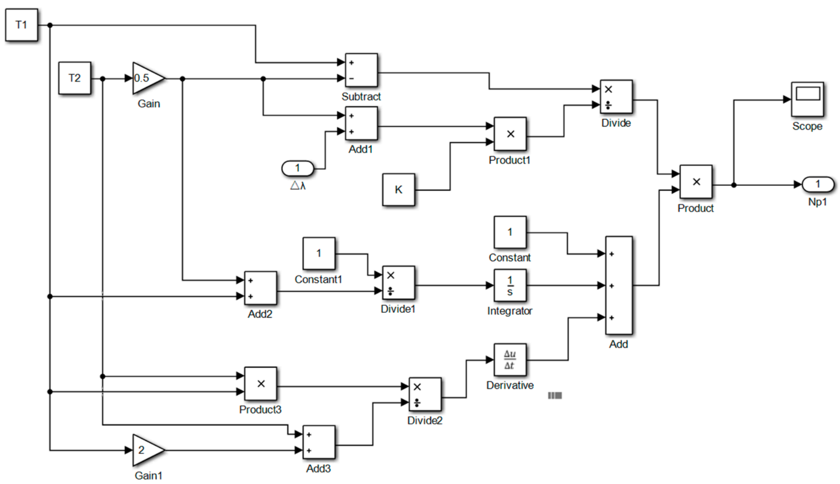

Figure 12. IMC controller internal structure simulation diagram.

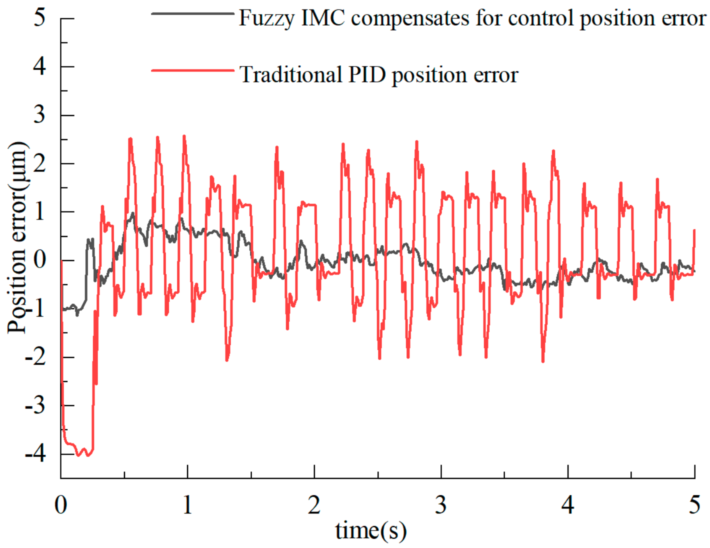

Figure 13. Output position error diagram of the hydraulic cylinder for the slope signal.

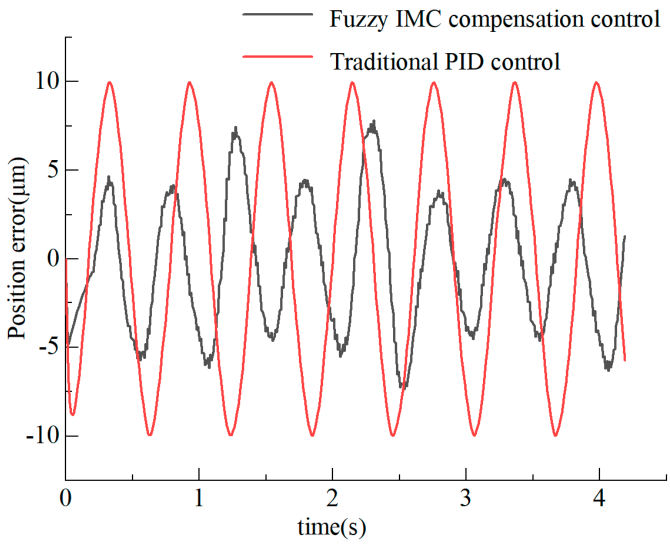

Figure 14. Position error curve of the sinusoidal signal system.

According to an analysis of Figure 13, the fuzzy IMC compensation control strategy can significantly improve the control accuracy of the pump-controlled AGC system position control, and the steady-state accuracy of the system can reach ± 0.7 μm. By analyzing Figure 14, it can be seen that the traditional PID control results in a large system position tracking error. The fuzzy IMC compensation controller shows a good following response, and its position following accuracy can reach around ± 1.8 μm.

5. Engineering Experiment Application

In order to verify the theoretical research results obtained in this paper, we took the enterprise research and development project "pump control servo system for lithium battery pole plate mill" as the experimental platform, as shown in Figure 15, and carried out corresponding experimental research on the nonlinear compensation control strategy proposed above with the pump control pole plate mill under fixed-roll-gap rolling conditions.

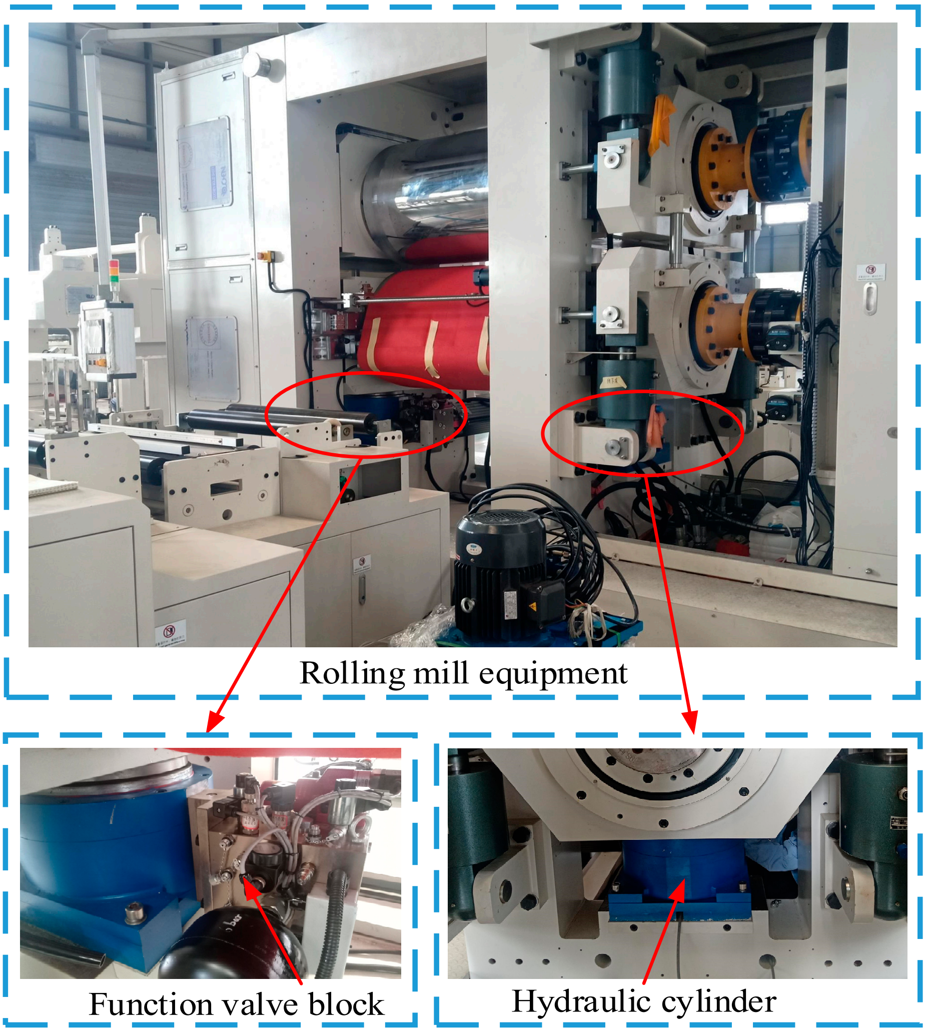

Figure 15. Pump control servo system experimental platform of a battery pole mill.

For the accuracy of the experiment, three kinds of 0.1 mm "S"-type slope trajectory displacement signals were used in this experiment, and the position and position error curves under the three displacement signals were obtained, as shown in Figure 16.

Through an analysis of Figure 16, it can be seen that the traditional PID control system has a large fluctuation in the position control of the hydraulic cylinder for different rolling conditions with a fixed roll gap, and the steady-state accuracy of the system is poor, which makes it difficult to ensure the rolling accuracy of the pole plate rolling through a set of control parameters. The steady-state error of the traditional PID control system after operation is ±0.005 mm when the displacement is 0.01 mm, ±0.006 mm when the displacement is 0.05 mm and ±0.008 mm when the displacement is 0.01 mm. Compared with traditional PID control, fuzzy IMC compensation control has no large position overshoot, the error of the steady-state position control accuracy under various displacements is within ±0.003 mm, and the time to steady state is faster than that of traditional PID control.

The target pole sheet thickness instructions of 140 μm, 150 μm, 200 μm and 300 μm were input through the system control interface, the thickness of the rolled pole sheet was measured by the laser thickness gauge and the obtained pole sheet thickness values were drawn into three-dimensional curves, as shown in Figures 17–20.

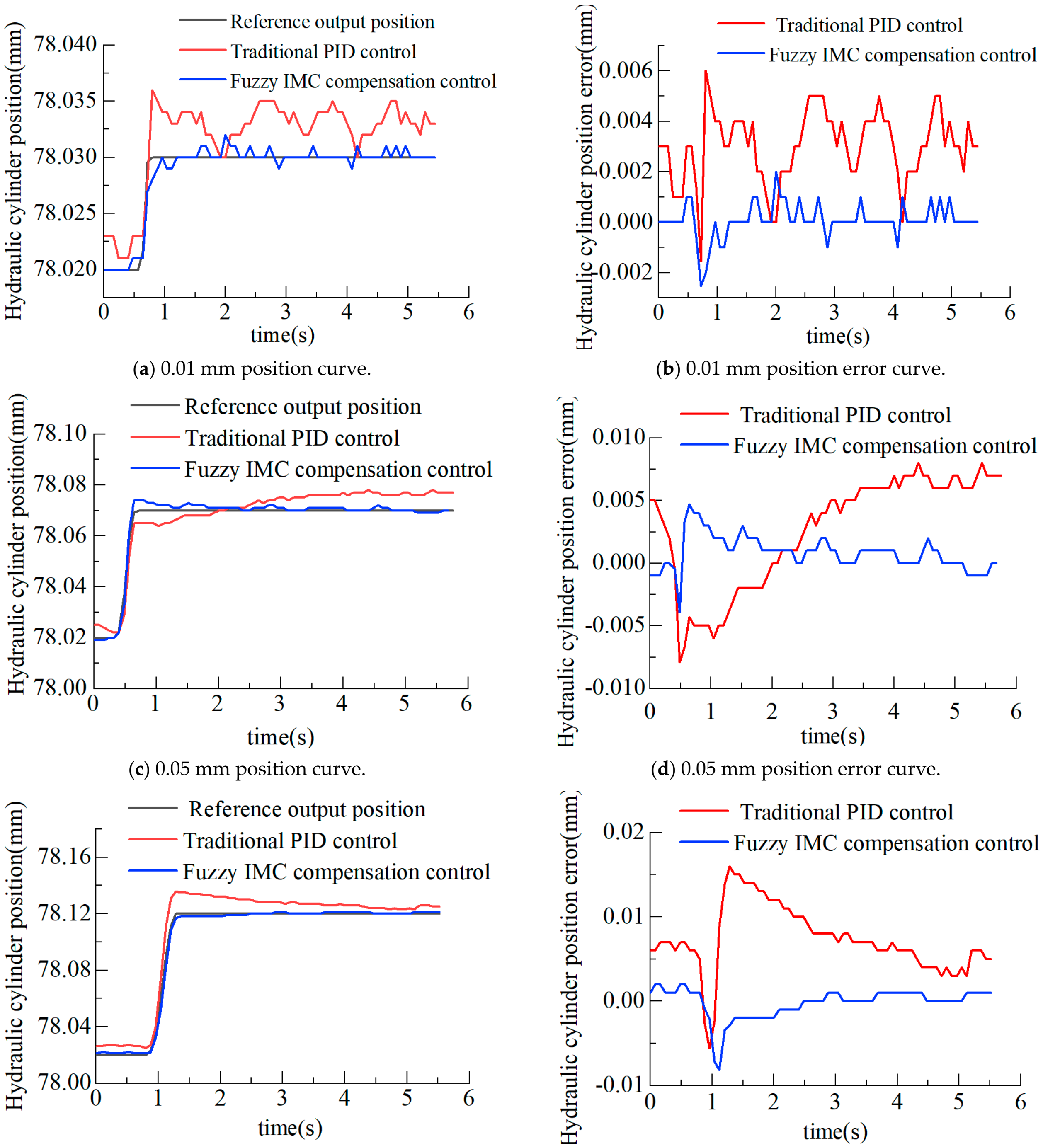

(**a**) 0.01 mm position curve. (**b**) 0.01 mm position error curve.

(**c**) 0.05 mm position curve. (**d**) 0.05 mm position error curve.

(**e**) 0.1 mm position curve. (**f**) 0.1 mm position error curve.

Figure 16. Experimental position curve and position error curve.

From Figures 17–20, it can be seen that the steady-state position error of the pump-controlled AGC system is ± 3 µm according to the displacement curve of the "S"-type slope trajectory, and the variation in the thickness of the roll forming is consistent with the change in the control instruction. Moreover, interference factors such as the force deformation of the roll in the rolling process and the gap error between the parts of the mill were not considered in this paper. Therefore, it can be considered that the fuzzy IMC compensation control algorithm can meet the control requirements of the automatic thickness control system of a pole plate rolling mill. The other main hydraulic components of the hydraulic system are listed in Table 2.

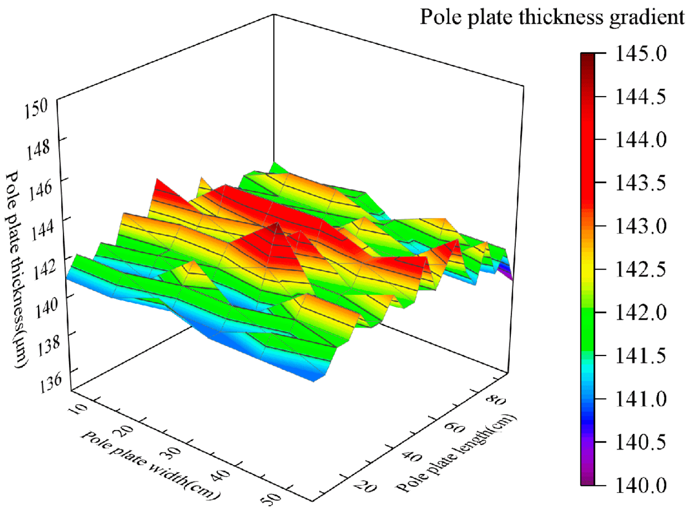

Figure 17. 140 μm negative electrode plate rolling.

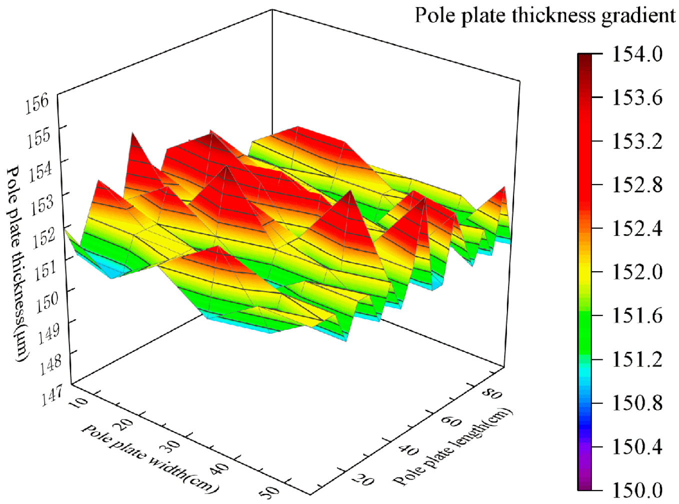

Figure 18. 150 μm negative electrode plate rolling.

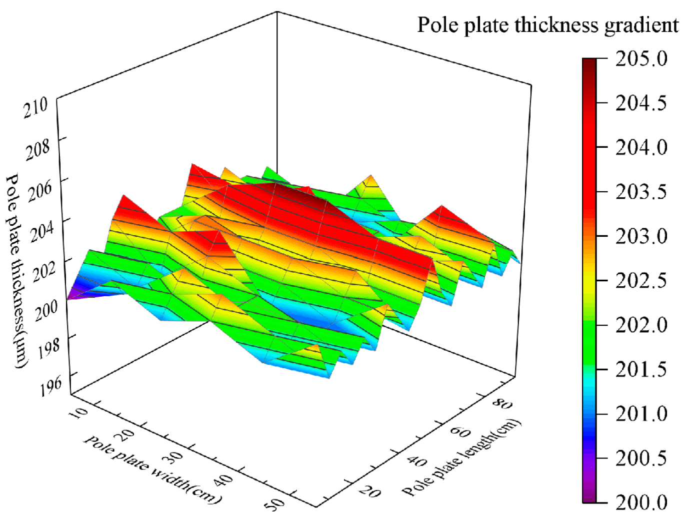

Figure 19. 200 μm negative electrode plate rolling.

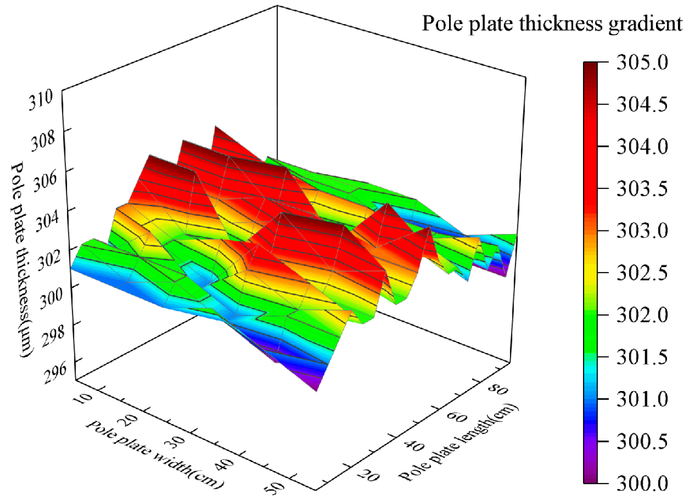

Figure 20. 300 μm negative electrode plate rolling.

Table 2. Hydraulic system main components details.

Name	Type	Manufacturers
Oil filter	DF ON 30 Q E 20 D 1.0	HYDAC
Two position three-way directional valve	DWDA-MAN-224	SUN
Check valve	CXED-XAN	SUN
Safety relief valve	RDBA-LCV	SUN
Two position two-way switch valve	DTDA-MCN-224	SUN

6. Conclusions

Based on the stiffness characteristics of pole plate rolling and the driving characteristics of the pump-controlled AGC, a fuzzy IMC compensation control strategy is proposed in this paper, which can effectively improve the precision of pump-controlled AGC position control. Its beneficial effects and limitations are mainly reflected in the following aspects:

Firstly, based on the nonlinear stiffness of the pole plate and the hydraulic cylinder, the nonlinear stiffness characteristics of the rolling process of the pole plate were studied and simulated.

Secondly, considering the influence of the nonlinear characteristics of the system on the thickness control of the pole plate, a compensation control strategy of the pole plate is proposed. Moreover, considering the load fluctuation caused by the uneven thickness of incoming material, fuzzy control combined with IMC control can solve the external load interference of the system. Combining the control advantages of the characteristic compensation controller and fuzzy IMC controller, the fuzzy IMC compensation control strategy is designed, and the simulation platform is built to simulate the system. The results show that the fuzzy IMC compensation controller can cope with the characteristic error and load disturbance of the system and improve the control precision and robustness of the system.

Finally, according to the research content of this paper, the project "pump control servo system of lithium battery pole mill" is used as the experimental platform. The accuracy of position control of the pump-controlled AGC system and automatic thickness control system of the pole plate mill are verified by experiments. The experimental results show that the fuzzy IMC compensation controller proposed in this paper can effectively improve the thickness forming accuracy of the pole plate mill. The pump-controlled AGC position control accuracy can reach within ±3 μm, and the roll forming thickness of the negative electrode sheet of the lithium battery can reach within ±5 μm, which ensures the rolling quality of the electrode sheet. The research results lay a theoretical and technical foundation for the popularization of electro-hydraulic pump control technology in the field of pole plate rolling. However, the limitation of this study is that it does not consider the deformation of the roll in the rolling process and the coupling between the components.

Author Contributions: Funding acquisition, G.C. and K.L.; formal analysis, K.W.; methodology, G.C. and K.W.; project administration, C.Z.; resources, G.C. and K.W.; software, K.W.; writing—original draft, K.W. and F.W.; writing—review and editing, K.W. and G.C.; supervision, K.W. and G.C. All authors have read and agreed to the published version of the manuscript.

Funding: This research was funded by the National Natural Science Foundation of China (Grant No. 52275066), the Natural Science Foundation of the Xinjiang Uygur Autonomous Region (2021D01A63), the Science and Technology Research Project of Colleges and Universities of Hebei Province (ZD2021340) and the Natural Science Foundation of the Xinjiang Uygur Autonomous Region (2022D01A51).

Institutional Review Board Statement: Not applicable.

Informed Consent Statement: Not applicable.

Data Availability Statement: Data are contained within the article.

Conflicts of Interest: The authors declare no conflicts of interest.

References

1. Xiao, Y.; Deng, S.; Liu, W.; Zhou, W.; Wan, F. Optimized Design of Battery Pole Control System Based on Dual-chip Architecture. *PLoS ONE* **2022**, *17*, e0264285. [CrossRef] [PubMed]
2. Meyer, C.; Weyhe, M.; Haselrieder, W.; Kwade, A. Heated Calendering of Cathodes for Lithium-Ion Batteries with Varied Carbon Black and Binder Contents. *Energy Technol.* **2020**, *8*, 1900175. [CrossRef]
3. Jiang, W.; Jia, P.; Yan, G.; Chen, G.; Ai, C.; Zhang, T.; Shen, W. Dynamic Response Analysis of Control Loops in an Electro-Hydraulic Servo Pump Control System. *Processes* **2022**, *10*, 1647. [CrossRef]
4. Yan, G.; Jin, Z.; Zhang, T.; Zhang, C.; Ai, C.; Chen, G. Exploring the Essence of Servo Pump Control. *Processes* **2022**, *10*, 786. [CrossRef]
5. Meyer, C.; Kosfeld, M.; Haselrieder, W.; Kwade, A. Process Modeling of the Electrode Calendering of Lithium-ion Batteries Regarding Variation of Cathode Active Materials and Mass Loadings. *J. Energy Storage* **2018**, *18*, 371–379. [CrossRef]
6. Xu, Y.X.; Niu, L.C.; Yang, H.; Xiao, Y.C.; Xiao, Y.J. Optimization of Lithium Battery Pole Piece Thickness Control System Based on GA-BP Neural Network. *J. Nanoelectron. Optoelectron.* **2019**, *14*, 978–986. [CrossRef]
7. Giménez, C.S.; Finke, B.; Nowak, C.; Schilde, C.; Kwade, A. Structural and Mechanical Characterization of Lithium-ion Battery Electrodes Via DEM Simulations. *Adcanced Powder Technol.* **2018**, *29*, 2312–2321. [CrossRef]
8. Giménez, C.S.; Finke, B.; Schilde, C.; Froböse, L.; Kwade, A. Numerical Simulation of the Behavior of Lithium-ion Battery Electrodes During the Calendaring Process Via the Discrete Element Method. *Powder Technol.* **2019**, *349*, 1–11. [CrossRef]
9. Sangrós Giménez, C.; Schilde, C.; Froböse, L.; Ivanov, S.; Kwade, A. Mechanical Electrical and Ionic Behavior of Lithium on Battery Electrodes Via DEM Simulations. *Energy Technol.* **2020**, *8*, 1900180. [CrossRef]
10. Park, K.; Myeong, S.; Shin, D.; Cho, C.W.; Kim, S.C.; Song, T. Improved Swelling Behavior of Li Ion Batteries by Microstructural Engineering of Anode. *J. Ind. Eng. Chem.* **2019**, *71*, 270–276. [CrossRef]
11. Duffner, F.; Kronemeyer, N.; Tübke, J.; Leker, J.; Winter, M.; Schmuch, R. Post-lithium-ion Battery Cell Production and its Compatibility with Lithium-ion Cell Production Infrastructure. *Nat. Energy* **2021**, *6*, 123–134. [CrossRef]
12. Maghareh, A.; Silva, C.E.; Dyke, S.J. Servo-Hydraulic Actuator in Controllable Canonical Form: Identification and Experimental Validation. *Mech. Syst. Signal Process.* **2018**, *100*, 398–414. [CrossRef]
13. Park, H.G.; Jeong, K.H.; Park, M.K.; Lee, S.H.; Ahn, K.K. Electro Hydrostatic Actuator System Based on Active Stabilizer System for Vehicular Suspension Systems. *Int. J. Precis. Eng. Manuf.* **2018**, *19*, 993–1001. [CrossRef]
14. Tri, N.M.; Binh, P.C.; Ahn, K.K. Power Take-off System Based on Continuously Variable Transmission Configuration for Wave Energy Converter. *Int. J. Precis. Eng. Manuf.-Green Technol.* **2018**, *5*, 103–110. [CrossRef]
15. Zhang, J.; Li, Y.; Xu, B.; Chen, X.; Pan, M. Churning Losses Analysis on the Thermal-hydraulic Model of a High-speed Electro-hydrostatic Actuator Pump. *Int. J. Heat Mass Transf.* **2018**, *127*, 1023–1030. [CrossRef]
16. Li, Y.H.; Ji, Z.L.; Yang, L.M.; Zhang, P.; Xu, B.; Zhang, J.H. Thermal-Fluid-Structure Coupling Analysis for Valve Plate Friction Pair of Axial Piston Pump in Electro-hydrostatic Actuator (EHA) of Aircraft. *Appl. Math. Model.* **2017**, *47*, 839–858. [CrossRef]
17. Zhang, J.; Chen, Y.; Xu, B.; Pan, M.; Chao, Q. Effects of Splined Shaft Bending Rigidity on Cylinder Tilt Behaviour for High-Speed Electrohydrostatic Actuator Pumps. *Chin. J. Aeronaut.* **2019**, *32*, 499–512. [CrossRef]
18. Lee, W.; Kim, M.J.; Chung, W.K. Asymptotically Stable Disturbance Observer-Based Compliance Control of Electro-hydrostatic Actuators. *IEEE/ASME Trans. Mechatron.* **2019**, *25*, 195–206. [CrossRef]

19. Antartis, D.; Dillon, S.; Chasiotis, I. Effect of Porosity on Electrochemical and Mechanical Properties of Composite Li-ion Anodes. *J. Compos. Mater.* **2015**, *49*, 1849–1862. [CrossRef]
20. Guan, Y.M.; Jiang, Z.; Zhao, F.H.; Qiu, Z.Z. Research on the Unevenness of Lithium Battery Plate and Structure Optimization Analysis of Roller Press. *Mech. Sci. Technol. Aerosp. Eng.* **2018**, *37*, 287–292.
21. Zad, H.S.; Ulasyar, A.; Zohaib, A. Robust Model Predictive Position Control of Direct Drive Electro-Hydraulic Servo System. In Proceedings of the 2016 International Conference on Intelligent Systems Engineering (ICISE), Islamabad, Pakistan, 15–17 January 2016; pp. 100–104.
22. Soon, C.C.; Ghazali, R.; Jaafar, H.I.; Hussien, S.Y.S. Sliding Mode Controller Design with Optimized PID Sliding Surface Using Particle Swarm Algorithm. *Procedia Comput. Sci.* **2017**, *105*, 235–239. [CrossRef]
23. Ren, G.; Esfandiari, M.; Song, J.; Sepehri, N. Position Control of an Electro-hydrostatic Actuator with Tolerance to Internal Leakage. *IEEE Trans. Control. Syst. Technol.* **2016**, *24*, 2224–2232. [CrossRef]
24. Cao, F. PID Controller Optimized by Genetic Algorithm for Direct-Drive Servo System. *Neural Comput. Appl.* **2020**, *32*, 23–30. [CrossRef]
25. Hong, W.; Wang, S.; Tomovic, M.M.; Liu, H.; Shi, J.; Wang, X. A Novel Indicator for Mechanical Failure and Life Prediction Based on Debris Monitoring. *IEEE Trans. Reliab.* **2016**, *66*, 161–169. [CrossRef]
26. Lu, C.; Wang, S.; Makis, V. Fault Severity Recognition of Aviation Piston Pump Based on Feature Extraction of EEMD Paving and Optimized Support Vector Regression Model. *Aerosp. Sci. Technol.* **2017**, *67*, 105–117. [CrossRef]
27. Li, X.; Jiao, Z.; Yan, L.; Cao, Y. Modeling and Experimental Study on a Novel Linear Electromagnetic Collaborative Rectification Pump. *Sens. Actuators A Phys.* **2020**, *309*, 111883. [CrossRef]
28. Fallahi, M.; Zareinejad, M.; Baghestan, K.; Tivay, A.; Rezaei, S.M.; Abdullah, A. Precise Position Control of an Electro-Hydraulic Servo System Via Robust Linear Approximation. *ISA Trans.* **2018**, *80*, 503–512. [CrossRef] [PubMed]
29. Wang, Z. *Research on Rolling Mechanism and Simulation of Battery Pole Sheet Roll*; Hebei University of Technology: Tianjin, China, 2018; pp. 12–13.
30. Zhou, J.; Wen, C.; Zhang, Y. Adaptive Output Control of Nonlinear Systems with Uncertain Dead-Zone Nonlinearity. *IEEE Trans. Autom. Control.* **2006**, *51*, 504–511. [CrossRef]
31. Song, J.Q.; Liu, X.J.; Tian, J.H. Multi-model internal model control method for steam generator water level control in nuclear power plant. *J. Taiyuan Univ. Sci. Technol.* **2014**, *35*, 166–170.
32. Chen, Y.T. Paper Quantitative Control based on fuzzy setpoint weighted IMC-PID Algorithm. *Packag. Eng.* **2018**, *39*, 157–162.